



Limb bud and flank mesoderm have distinct “physical phenotypes” that may contribute to limb budding

Brooke J. Damon^{a,1}, Nadejda V. Mezentseva^{b,1}, Jaliya S. Kumaratilake^{b,c},
Gabor Forgacs^{a,d,*}, Stuart A. Newman^{b,*}

^a Department of Physics and Astronomy, University of Missouri-Columbia, Columbia, MO 65211, USA

^b Department of Cell Biology and Anatomy, New York Medical College, Valhalla, NY 10595, USA

^c Discipline of Anatomical Sciences, University of Adelaide, Adelaide, SA 5005, Australia

^d Department of Biological Sciences, University of Missouri-Columbia, Columbia, MO 65211, USA

ARTICLE INFO

Article history:

Received for publication 17 October 2007

Revised 9 May 2008

Accepted 4 June 2008

Available online 20 June 2008

Keywords:

Limb bud

Surface tension

Active response

α -smooth muscle actin

ABSTRACT

Limb bud outgrowth in chicken embryos is initiated during the third day of development by Fibroblast Growth Factor 8 (FGF8) produced by the newly formed apical ectodermal ridge (AER). One of the earliest effects of this induction is a change in the properties of the limb field mesoderm leading to bulging of the limb buds from the body wall. Heintzelman et al. [Heintzelman, K.F., Phillips, H.M., Davis, G.S., 1978. Liquid-tissue behavior and differential cohesiveness during chick limb budding. *J. Embryol. Exp. Morphol.* 47, 1–15.] suggested that budding of the limbs is caused by a higher liquid-like cohesivity of limb bud tissue compared with flank. We sought additional evidence relevant to this hypothesis by performing direct measurements of the effective surface tension, a measure of relative tissue cohesivity, of 4-day embryonic chicken wing and leg bud mesenchymal tissue, and adjacent flank mesoderm. As predicted, the two types of limb tissues were 1.5- to 2-fold more cohesive than the flank tissue. These differences paralleled cell number and volume density differences: 4-day limb buds had 2- to 2.5-fold as many cells per unit area of tissue as surrounding flank, a difference also seen at 3 days, when limb budding begins. Exposure of flank tissue to exogenous FGF8 for 24 h increased its cell number and raised its cohesivity to limb-like values. Four-day flank tissue exhibited a novel and unique active rebound response to compression, which was suppressed by the drug latrunculin and therefore dependent on an intact actin cytoskeleton. Correspondingly, flank at this stage expressed high levels of α -smooth muscle actin (SMA) mRNA and protein and a dense network of microfilaments. Treatment of flank with FGF8 eliminated the rebound response. We term material properties of tissues, such as cohesivity and mechanical excitability, the “physical phenotype”, and propose that changes thereof are driving forces of morphogenesis. Our results indicate that two independent aspects of the physical phenotype of flank mesoderm can be converted to a limb-like state in response to treatment with FGF8. The higher tissue cohesivity induced by this effect will cause the incipient limb bud to phase separate from the surrounding flank, while the active mechanical response of the flank could help ensure that the limb bud bulges out from, rather than becoming engulfed by, this less cohesive tissue.

© 2008 Elsevier Inc. All rights reserved.

Introduction

The morphogenesis of the vertebrate limb begins with the bulging of the limb buds from the body wall at four sites along the embryo's surface. In the avian embryo, the lateral plate mesoderm is induced by paraxial signals (Saito et al., 2006) to generate limb buds at the axial levels of the cervical-thoracic (forelimb or wing) and lumbosacral (hindlimb or leg) somites by the third day of development (Nowicki et

al., 2003). The mesenchymal cells of the limb buds and adjacent flank are spatially homogeneous and morphologically similar until sub-populations within the limb buds begin to condense into cartilaginous primordia and pre-muscle masses more than a day later.

Exposure of the limb field mesoderm to Fibroblast Growth Factor-8 (FGF8) and/or other FGFs secreted from the apical ectodermal ridge (AER) is essential in promoting limb bud outgrowth (Mahmood et al., 1995; Vogel et al., 1996; Crossley et al., 1996; Ohuchi et al., 1997; Lewandoski et al., 2000; Moon and Capecchi, 2000; Sun et al., 2002). The limb vs. flank difference, however, is manifested in avian and mammalian species even earlier than the initial bulging (Min et al., 1998; Xu et al., 1998; Sekine et al., 1999; Kawakami et al., 2001; Agarwal et al., 2003; Tanaka and Tickle, 2004; Saito et al., 2006).

* Corresponding authors. G. Forgacs is to be contacted at Department of Physics and Astronomy, University of Missouri-Columbia, Columbia MO 65211, USA.

E-mail addresses: forgacs@missouri.edu (G. Forgacs), newman@nymc.edu (S.A. Newman).

¹ These authors contributed equally to this work.

How might changes in the limb field cells lead to bulging of the tissue from the surrounding flank? Much evidence suggests that on the time scale of typical morphogenetic processes many embryonic tissues behave similarly to viscous liquids. As a consequence, they exhibit characteristic liquid mechanical properties, including rounding up into droplet-like spheres, cohesivity and surface tension, and coalescence and miscibility/immiscibility (Steinberg and Poole, 1982; Armstrong, 1989; reviewed in Forgacs and Newman, 2005). Based on these ideas and indirect evidence from cell sorting and tissue fragment coalescence experiments, Phillips and his coworkers (Heintzelman et al., 1978) made the novel suggestion that limb budding occurs because limb field mesoderm becomes more cohesive than the somatopleural mesoderm from which it arises. According to this hypothesis, a limb bud would emerge from the body wall by a physical process akin to that which causes a droplet of water to separate and protrude from the surface of a pool of oil.

Recently, compression tensiometry for measuring the biomechanical properties of tissues directly has become available (Foty et al., 1996; Forgacs et al., 1998; Hegedús et al., 2006; Norotte et al., 2008). In this method, small fragments of the tissue are allowed to round up in suspension culture, compressed between parallel plates and let to return to mechanical equilibrium. During the compression and subsequent relaxation process, forces exerted by the tissue on the plates, as well as the tissue's exact shape, are monitored. The analysis of the force–time curve by well-established physical models provides reproducible values for the tissue's surface tension and viscoelastic parameters (Forgacs et al., 1998; reviewed in Forgacs and Newman, 2005; Norotte et al., 2008).

We have utilized these methods to further test the plausibility of the hypothesis of limb budding of Heintzelman et al. (1978). Here we report that at 4 days of development both wing and leg bud mesenchyme had higher surface tensions (i.e., were more cohesive) than flank tissue. The magnitude of the difference between limb and flank was similar to that measured in other pairs of embryonic tissues which behaved like immiscible liquids (Foty et al., 1996). A cellular correlate of the observed cohesivity difference between flank and limb mesoderm is the difference in cell density, which we show by morphometric analysis to be more than twice the flank value in limb buds, both at 4 days, when the compression experiments were performed, and at 3 days, when limb budding is initiated. Significantly, in relation to the hypothesis of Heintzelman et al. (1978), we found that exogenous application of FGF8 induced the flank mesoderm to increase its cell number, and to bring its surface tension to a value within the range of the limb bud mesoderms.

In the course of these studies we discovered that the flank mesoderm (which contains no myoblasts at these stages), exhibited an unusual active mechanical response during the first two minutes of compression, manifested by a sudden increase of the force exerted by the tissue on the compression plate. This rebound response has not been reported in any of the more than a dozen embryonic tissue types and aggregates of genetically modified tissue culture cells analyzed in the same fashion in earlier studies (Foty et al., 1996; Forgacs et al., 1998; Duguay et al., 2003). We found it to be dependent on an intact actin cytoskeleton in flank tissue, and correlated with high levels of expression of α -smooth muscle actin (SMA) (compared to trace amounts in the limb buds) and an extensive network of cytoplasmic microfilaments. Treatment with FGF8 elevated the cohesivity of the flank to limb-like values and completely eliminated the rebound response. However, the low cohesivity of flank tissue relative to limb bud was not due to the cytoskeletal features responsible for the rebound response, since elimination of the latter by treatment with the drug latrunculin had no effect on the tissue's cohesivity.

We conclude that cohesivity (high in limb bud, low in flank) and the ability to mount an active mechanical response (absent in limb bud, present in flank) are two independent features of the “physical phenotype” of these tissues (see also Newman and Comper, 1990). Changes toward limb-like values in each of these features are induced

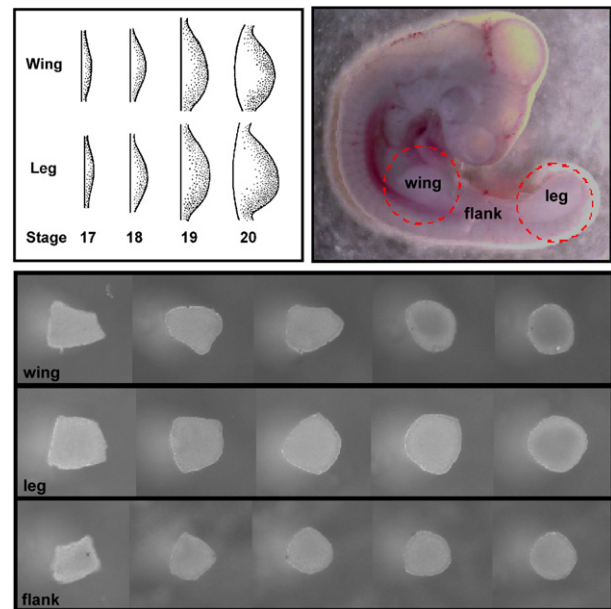


Fig. 1. (Top left) Changes in the shape of chicken wing and leg buds as the limb buds emerge from the flank between HH17 (~58 h) and HH20 (~71 h). (Redrawn from Hamburger and Hamilton, 1951, with modifications.) (Top right) E4 (HH23) chicken embryo, showing sources of tissue used in this study. (Bottom) The rounding of fragments (~300 μ m) of E4 leg, wing and flank tissue occurs within 24 h in vitro, an indication of their liquid-like behavior. The fragment in the left-most panel of each row was photographed shortly after explantation. The fragments were photographed successively 5 h, 11.5 h, 17.5 h and 24 h later.

by FGF8 and both plausibly contribute to the induction of limb buds from the flank tissue during embryogenesis.

Materials and methods

Embryos, tissues and reagents

Fertilized White Leghorn eggs (Ozark Hatcheries, Neosho, MO for tensiometry experiments, Moyers Chicks, Quakertown, PA for histologic, ultrastructural, and DNA and RNA analyses) were incubated at 38.5 °C with 80% humidity until Hamburger–Hamilton stage HH23 (Hamburger and Hamilton, 1951) was reached (4 days, Fig. 1, upper right panel). Dissections of wing and leg buds, and flank (somatopleural) tissue between them, were performed in cold (21–23 °C) Earle's Balanced Salt Solution without calcium or magnesium (EBSS, Invitrogen). A solution of EBSS with 2 mM ethylene diamine tetra-acetic acid (EDTA, Invitrogen) was used to chelate calcium, allowing layers of ectodermal cells to be gently removed. The action of the EDTA was halted using a solution of EBSS with 1.8 mM CaCl_2 and 0.8 mM MgSO_4 + 10% Fetal Bovine Serum (EBSS+FBS, Invitrogen). Tissue explants were cut into ~300 μ m fragments and incubated where indicated for ~24 h in Dulbecco's Modified Eagles Medium containing 1% Penicillin Streptomycin (DMEM, Invitrogen). FBS (10%) was added to the medium for all tensiometric and some other assays, as indicated. Recombinant mouse fibroblast growth factor 8b (FGF8b, R&D Systems) was used at a concentration of 25 ng/ml and latrunculin A (Invitrogen) at 1 μ M. Trypan blue, used in the post-compression viability assay, was purchased from Invitrogen.

Tensiometry

Incubation in the presence of FBS caused the tissue fragments to round into spheres (Fig. 1, bottom). Tissue surface tension was measured with an in-house built compression plate tensiometer (Fig. 2, left). The tensiometer's inner chamber is maintained at 37 °C and contains CO_2 independent medium with 10% FBS and 1% penicillin

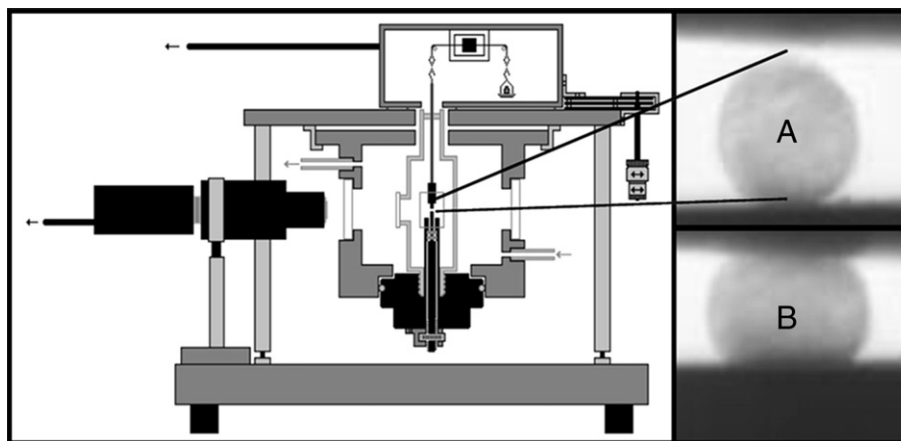


Fig. 2. (Left), A schematic of the tensiometry apparatus (not to scale). A video camera is used to capture the image of the compressed explant of intact tissue and a microbalance measures the force with which the explant resists the compressive load. A water jacket maintains the inner chamber at 37 °C. (Right), Images of the tissue explant before the compression (A) and during the compression (B).

streptomycin (CO₂I, Invitrogen). A typical measurement of the effective surface tension of a living tissue is performed as follows: a tissue spheroid (~300 μm diameter) is placed in the inner chamber of the tensiometer on the lower compression plate and uniaxially compressed to a fixed strain (Fig. 2, right). To minimize adhesion, plates were coated with poly (2-hydroxyethylmethacrylate) (poly-HEMA) (Folkman and Moscona, 1978). The shape of the compressed explant before, during and after compression was recorded with a Spot Insight CCD camera (Diagnostic Instruments, Sterling Heights, MI) fitted to a horizontally positioned dissecting microscope (SZ60, Olympus). A Cahn 2000 Microbalance (Cahn Instruments, Inc., Cerritos, CA), controlled with Labview software (National Instruments, Austin, TX) recorded the time variation of the applied compressive load. To avoid irreversible damage to tissues, explants were compressed a maximum of 30% of their original diameter. The relaxation process was followed until the compressive force reached a constant equilibrium value (typically after 30–45 min), at which point the plates were separated, and the explant was allowed to regain its original shape. The rare cases where this did not occur were discarded. Tensiometry was carried out on six independent samples for each tested tissue group (i.e., a total of 30 samples). Samples for each preparation were drawn from separate lots of embryos, with measurements performed on different days.

In order to verify that these tissue explants indeed are analogous to liquids in that their surface tension is independent of the extent of compression, explants were compressed twice with varying magnitude of the compressive force (30 min of recovery time in the uncompressed state was allowed between successive measurements).

The surface tension of the tissue was evaluated using the Laplace equation, $F_{eq}/(\pi R_3^2) = \sigma(1/R_1 + 1/R_2)$ (Israelachvili, 1992). Here σ is the tissue's apparent surface tension (i.e. interfacial tension with the surrounding tissue culture medium), F_{eq} is the equilibrium value of the compressive force, R_3 is the radius of the circular contact area of the compressed explant with the plates. R_1 is the radius of curvature of the explant's surface along its equatorial plane and R_2 is the curvature of its profile, assumed to be circular between the plates.

Trypan blue exclusion test

After measurements were performed, the trypan blue exclusion test was utilized to determine if the cells near the surface of the tissue explants were viable. Additionally, explants were cut in half to determine if necrotic cells were present within their interiors. The tissue explants were allowed to soak in a droplet of DMEM containing 20% trypan blue stain for 10 min. Trypan blue was then diluted, the explant was placed

into a Petri dish containing fresh DMEM and observed under the microscope. Explants contained a minimal number (<5%) of dead cells.

Determination of mesenchyme cell density

Mesenchyme cell volume density and cell number density were determined on semi-thin (1 μm) resin sections stained with Toluidine blue stain. Each parameter was determined on sections obtained from somatopleure (flank fold), wing bud and leg bud regions of E3 and E4 embryos, and from wing and flank explants freshly isolated from E4 embryos and E4 flank incubated for 24 h in the absence and presence of 25 ng/ml FGF8b. Three sections each from each of four E3 and E4 embryos, and from each of four explants of the five different preparations, were analyzed. Four random fields from each section were used for cell volume density and cell number density (i.e., number per 500 μm²) determinations.

Cell volume density (V_v) was determined by point counting (Weibel et al., 1966) using a 100 point graticule in a 10× eye-piece with a 40× objective. Points falling on endothelial cells of blood vessels, red blood cells or the ectoderm cells were not counted. To determine mesenchyme cell numbers per 500 μm², digital images were obtained at 10×40 magnification and the area occupied by cells was determined using the NIH Image J computer program. Then the same area was printed and the cell number was counted manually. Thin cell processes, endothelial cells of blood vessels, red blood cells and ectoderm cells were not counted. For some of the tissue samples cell volume and number densities were also evaluated automatically using the NIS-Elements BR program (Nikon), with results virtually identical to those obtained by the manual method.

Quantitative real-time PCR

For determination of relative increase in flank tissue cell number in response to FGF8 treatment, entire flank regions were dissected from 4-day embryos and incubated either in DMEM or DMEM + 25 ng/ml FGF8b for 24 h, as described above. Eight samples of treated and control tissues, consisting of 5 flanks each, were used for DNA determination. This comparison was made separately for flanks incubated in the absence and presence of 10% FBS. DNA was extracted from each sample using the QIAamp DNA mini kit (Qiagen). Isolated DNA was used directly for comparative quantitative PCR with β-actin primers (see below). For determination of relative gene expression of actin isoforms, total RNA was extracted from 4-day chicken embryo legs buds, wing buds and flanks by using the RNeasy kit according to manufacturer's protocol (Qiagen). Three different RNA samples were generated for each

tissue type. Total (RNA 500 ng) was used for reverse transcription in a 20- μ l reaction with oligo(dT)₁₈ and AMV (Fisher) at 42 °C for 1 h. qPCR reactions were in 20 μ l with 1 μ l of cDNA, 10 μ l of 2 \times Brilliant SYBR Green 2 \times master mix (Stratagene), and 150 nM forward and reverse primers. The qPCR reactions were performed by using the Mx3005P Real-Time qPCR instrument (Stratagene). The reaction conditions were 95 °C for 10 min, then 35 cycles of 95 °C for 30 s, 55 °C for 1 min and 72 °C for 30 s. Emitted fluorescence was measured once at the end of extension (72 °C). The threshold cycle (Ct) was determined as the mean of three biological replicates by using the adaptive baseline algorithm in the MX3005P software package. Analysis was performed on the data output using Origin 8 (OriginLab, Northampton, MA). All measurements were normalized to GAPDH expression and analyzed by the “delta delta Ct” method (Livak and Schmittgen, 2001). Primers pairs were as follows: chicken α -actin (NM_001031229), sense: TGGATTGAGGCTC-TATTCTTG, antisense: TTGCGGTGAACGATGGATGG (product size 101 base pairs); chicken β -actin (NM_205518), sense: CCGTACCAAT-TACTGGTGTAGATG, antisense: GCCTTCATTCACATCTATCACTGG (product size 163 base pairs); chicken GAPDH (AF047874), sense: CCACTGGTGTCTTACCACC, antisense: GGCAGCACCTTGCCATCTC (product size 317 base pairs).

Immunoblot analysis

Leg and wing buds, and flanks, were lysed in Lysis-M solution containing Complete inhibitor (Roche). Protein concentration was measured by the BCA method (Pierce). Samples containing equal amounts of protein were loaded into SDS 4–20% Tris–HCl Criterion gel (Bio-Rad). Proteins were transferred to nitrocellulose membrane (Bio-Rad) by electroblotting for 1 h in Tris–Glycine/20% methanol. Membranes were blocked for 1 h at room temperature in 3% nonfat milk (Bio-Rad)+TTBS (Tris buffered saline, 0.1% Tween), then incubated overnight at 4 °C with primary antibody diluted in blocking solution. Blots were washed in TTBS, incubated for 1 h with secondary antibody and washed again in TTBS. Signal was visualized by means of HRP ECL western blotting substrate (Pierce). Primary antibodies were directed against the N-terminus of human smooth muscle α -actin (Abcam ab 5694; dilution 1:500) and β -actin (Abcam ab 6276; dilution 1:2000), which was used as a loading control. Secondary antibodies were goat anti mouse-horseradish peroxidase (HRP) (Jackson Immunoresearch) or goat anti rabbit-HRP (Santa Cruz). The dilution of the secondary antibodies was 1:5000.

Immunohistochemistry

Chicken embryos at 4 days of incubation (E4) were fixed for 12–18 h in 4% paraformaldehyde prepared in 0.1 M phosphate buffered saline (PBS) with 8% sucrose (pH 7.4). The trunk (just inferior to the heart, extending to the tail bud) of the embryo was dissected horizontally into three segments: those including the wing and leg

buds, and the flank segment in between. Each segment was dehydrated through a graded series of ethanol and embedded in paraffin wax.

Sections (10 μ m) were mounted onto glass slides, de-waxed, incubated for 30 min with 0.02 M glycine followed by another 30 min incubation with blocking solution (2% normal goat serum, 1% bovine serum albumin, 0.1% Triton X-100, 0.05% Tween 20, in PBS). Sections were then incubated overnight at 4 °C with primary antibody directed against smooth muscle α -actin (Abcam ab5694, 1:1800 dilution) followed by the secondary antibody (CY3-conjugated goat anti-rabbit IgG, Jackson Immunoresearch; 1:500) for 90 min at room temperature. After the incubation with each antibody, the sections were subjected to 3 \times 5 min washes with the blocking solution. After the last wash, cover-slips were mounted using 50% glycerol in PBS. Some sections were incubated with the blocking solution in place of the primary antibody and used as the control. All sections were examined in a fluorescence microscope with the CY3 filter set. Images were photographed with a digital camera using the same exposure time for all sections. All results were consistent among three embryos.

Electron microscopy

Chicken embryos (E3 and E4) or incubated E4 flank tissues were fixed overnight (16–18 h) at 4 °C with a chilled fixative containing 5% glutaraldehyde, 4% paraformaldehyde, 8% sucrose and 2 mM CaCl₂ prepared in 0.1 M cacodylate buffer with a final pH of 7.4. The trunk of the embryo was dissected into wing bud, leg bud and flank segments as above. Each part was post-fixed in 1% osmium tetroxide for 1 h, dehydrated through a graded series of ethanol, embedded in Spurr's resin and polymerized at 60 °C. Semi-thin (1 μ m) sections were cut, stained with toluidine blue and used for selection of the appropriate areas. Thin sections (silver in interface) were cut using a diamond knife, mounted on copper grids, stained with uranyl acetate and lead citrate and examined in Jeol or Hitachi electron microscopes. All reported results were consistent among at least three embryos or tissue fragments.

Statistical analysis

For the tensiometric, morphometric and qPCR experiments, data were analyzed by ANOVA with values of α and p as specified in the Figure and Table legends, followed by the Tukey two-way multi-comparison test.

Results

Cohesivity and cellular density of limb and flank tissues

Our goal was to compare properties of limb and flank as close as possible to the stage of embryonic development when budding is

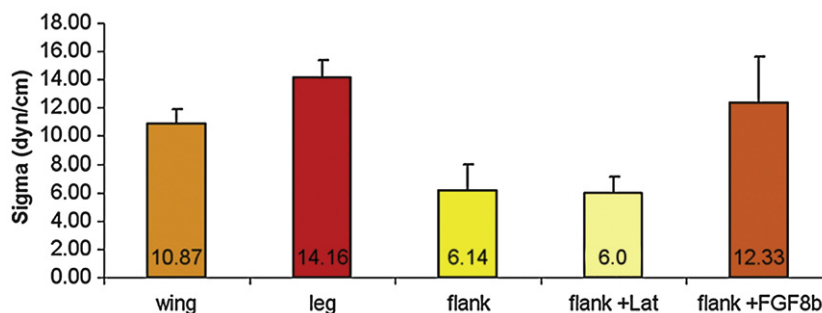


Fig. 3. Surface tensions (dynes/cm) measured for spherical explants of intact E4 mesenchyme: wing, leg, flank (wing vs. flank, $p < 0.0003$; leg vs. flank, $p < 0.0001$; wing vs. leg, $p < 0.0005$), flank incubated with 1 μ M latrunculin A (Lat) (flank vs. flank + Lat, N.S.), and flank incubated with 25 ng/ml FGF8b (flank vs. flank + FGF8b; $p = 0.003$, wing vs. flank + FGF8b, N.S.; leg vs. flank + FGF8b, N.S.). Error bars indicate the SD. Six different explants were measured separately for each test group.

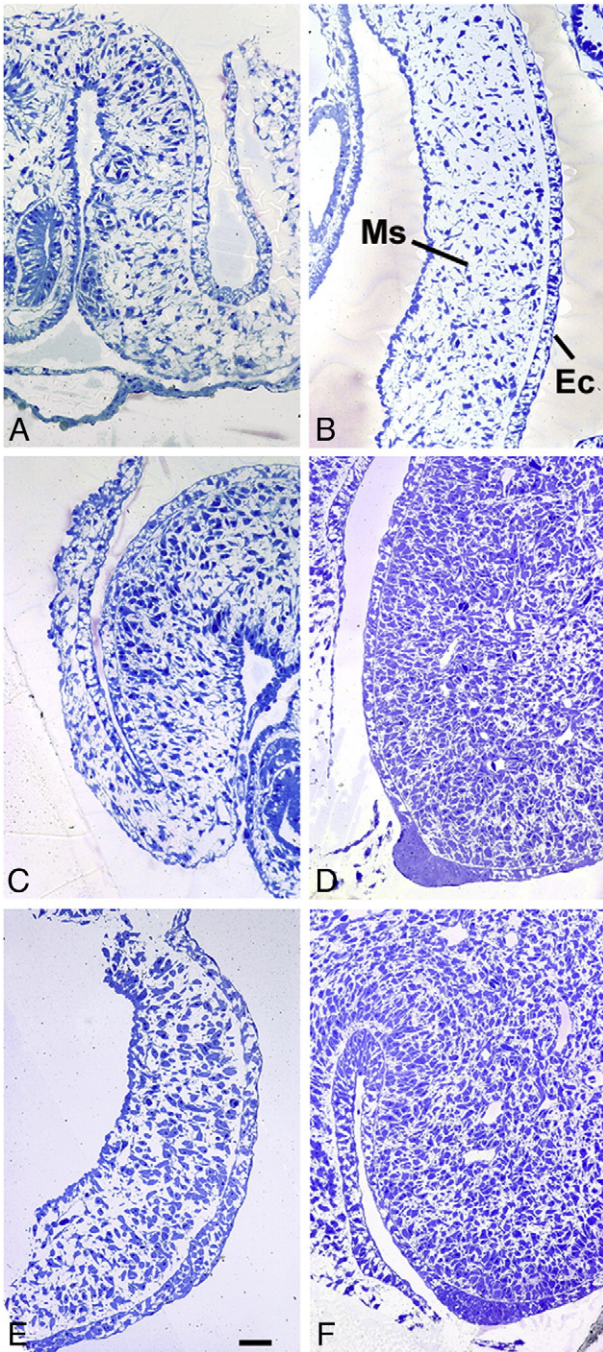


Fig. 4. Resin-embedded semi-thin sections of flank, leg bud and wing bud from E3 (A, C, E) and E4 (B, D, F) chicken embryos stained with Toluidine blue. A, B: flank; C, D: leg bud; E, F: wing bud. Ms: mesenchyme; Ec: ectoderm. Scale bar=20 μ m.

initiated. While the flank can be induced to form limbs or limb-like structures up until at least HH18 (3 days of development; E3) (Vogel et al., 1996; Min et al., 1998), during the period when the normal limb buds first begin to emerge (Fig. 1, upper left), it was technically infeasible to perform tensiometry on limb and flank tissues at this early stage embryogenesis. We therefore did our measurements at the end of the fourth day (HH23; E4).

Explants comprising tissue fragments isolated from the flank, and leg and wing limb buds, of E4 embryos (Fig. 1, upper right) round up to form spheres within 24 h when incubated while suspended in culture medium (Fig. 1, bottom), an indication of their liquid-like behavior (Forgacs and Newman, 2005). No extensive necrosis of cells was seen in these spherical explants, after the tensiometry measurements were

Table 1

Cell volume density and number density of E3 and E4 flank and limb bud mesenchyme

	Volume density (cell per tissue)			Number density (cell number per 500 μ m ²)		
	Flank	Wing	Leg	Flank	Wing	Leg
E3	15.92±1.87	37.06±2.24	30.42±4.06	2.02±0.25	4.73±0.32	4.62±0.36
E4	15.84±1.55	39.81±3.00	44.2±1.55	2.34±0.19	5.23±0.42	6.22±0.24

Volume density of mesenchymal cells was significantly different between flank and wing and leg buds ($\alpha=0.001$, $p=0.001$) for both E3 and E4. Leg bud tissue was the only one of the three for which Vv increased significantly between the third and fourth day of development ($\alpha=0.03$, $p=0.012$). Cell number density was significantly different between flank and buds ($\alpha=0.001$, $p=0$) for both E3 and E4. The number density of mesenchymal cells in leg buds significantly increased during development from E3 to E4 ($\alpha=0.005$, $p=0.004$). See Materials and methods for statistical test used.

completed, by the trypan blue exclusion test. In addition, it was observed that upon release of the compressive load samples would eventually regain their original spherical shape, suggesting that cell motility was not affected by the compression.

Surface tension measurements of spherical explants of E4 leg, wing and flank tissue (Fig. 2) showed that mesenchyme of both limb bud types are more cohesive than flank tissue, with leg bud being more cohesive than wing bud (Fig. 3) in agreement with previous qualitative studies (Heintzelman et al., 1978). There were significant differences between wing and flank ($p<0.003$), leg and flank ($p<0.0001$), and wing and leg ($p<0.0005$) surface tension values.

Semi-thin sections of wing and leg buds of E3 and E4 embryos showed that these tissues had a higher density of cells compared to the corresponding flanks (Fig. 4). Quantitation of cell volume density and number density showed E4 wing bud having 2.51× and 2.24× the flank values, and leg bud having 2.79× and 2.66× the flank values of the respective parameters. At E3, when limb budding is initiated, the corresponding ratios for the cell volume fraction and number density relative to flank were 2.33 and 2.34 for wing bud and 1.91 and 2.29 for leg bud (Table 1). Thus, from the start of limb budding, continuing for at least a full day, limb bud mesenchyme has 2–3 fold more cells per unit volume of tissue than flank mesenchyme.

Since interpretable data from the tensiometric assays could only be obtained from compression of spherical tissue fragments, as described above, explants were required to be incubated in a rotary shaker for 24 h before the measurements were performed. Moreover, explants from E3 embryos were too small to be analyzed by our methods, so E4 embryos were used in these assays. To determine if the density differences seen in the freshly isolated limb and flank explants persisted after this incubation step and could thus have contributed to the measured differences in the physical phenotype of the explants, we fixed E4 wing bud and flank tissues immediately after explantation and after the 24 h incubation. We found that the freshly isolated explants differed in the expected fashion, with wing bud cell volume and number densities about 1.5 times those of the flank, but the absolute values of these quantities were 1.5 to 2× higher than those seen in E4 wing and flank tissues fixed in situ (Tables 1 and 2). As

Table 2

Cell volume density and number density of E4 flank and wing bud explants

	Volume density (cell per tissue)		Number density (cell number per 500 μ m ²)	
	Flank	Wing	Flank	Wing
0 h	36.75±2.35	54.65±2.24	6.08±0.28	9.68±0.66
24 h	26.52±2.26	55.41±2.40	3.78±0.26	8.46±0.62
24 h+FGF8	36.61±3.23	N.D.	3.57±0.5	N.D.

At 0 h and 24 h mesenchymal cell volume and number densities were significantly different between E4 explants of wing bud and untreated flank ($\alpha=0.001$; $p=0$). Cell volume density, but not cell number density, differed significantly ($\alpha=0.05$; $p=0.046$) between 24 h untreated flank explants and 24 h FGF8-treated flank. N.D., not determined.

neither the cells themselves, nor their nuclei or mitochondria, showed signs of shrinkage in these fixed explants (not shown), the elevated density values suggest that both the limb and flank ECMs responded differently to the fixative in the explants (which had free mesenchymal surfaces exposed), than in the embryos (where the mesenchyme is surrounded by ectoderm). (Note that tensiometry was performed on living tissues, which would not have experienced shrinkage relative to the *in situ* state.) After 24 h of incubation the limb and flank tissues retained their disparity in both cell volume and number densities, although the flank Vv value fell by about 28% during this step (Table 2).

Rebound response of flank tissue

The force relaxation data for flank tissue explants demonstrated an active mechanical response (Fig. 5), generally within a minute after the application of the compressive load. Apart from this rebound response, the relaxation curves in Fig. 5 are typical for viscoelastic materials, in which a rapid, more elastic response to deformation is followed by a slower, liquid-like viscous response (Fung, 1990; Shaw et al., 2004).

Following the active response, the compression force ultimately relaxes to an equilibrium value (Fig. 5), allowing the surface tension

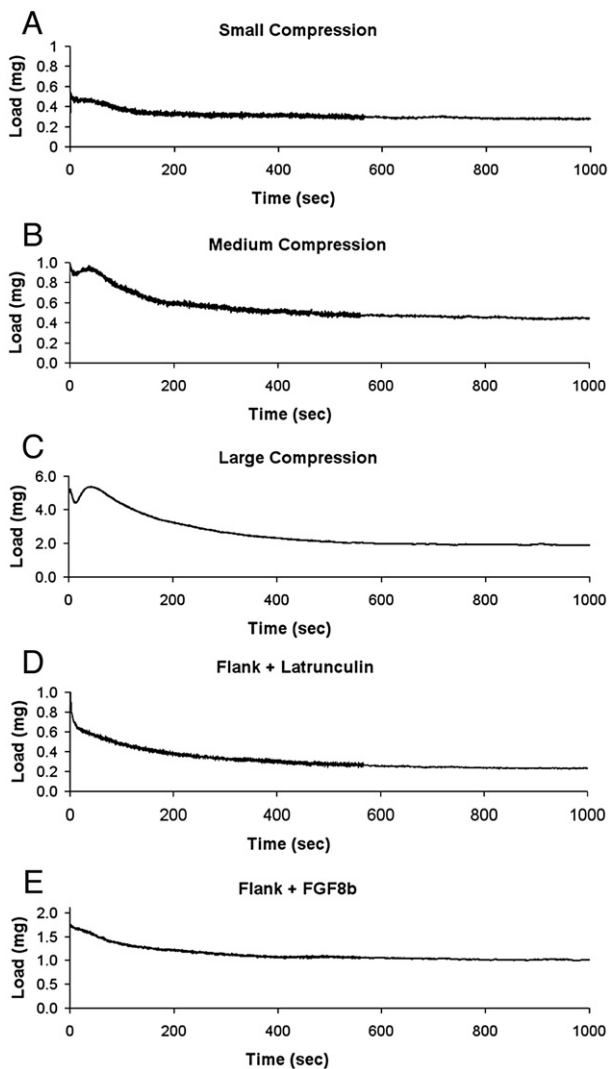


Fig. 5. Compression force relaxation in E4 flank tissue explants. (A–C) active response increasing with the magnitude of the initial load; (D) effect of treatment for 30 min with 1 μ M latrunculin immediately prior to compression; (E) effect of treatment with 25 ng/ml exogenous FGF8b during the 24 h rounding process.

Table 3
Actin isoform expression in E4 flank and limb bud tissues

	Flank	Leg	Wing
β -actin	0.98 \pm 0.4	0.79 \pm 0.17	1.42 \pm 0.64
α -actin (SMA)	$2 \times 10^{-3} \pm 6 \times 10^{-4}$	$4.5 \times 10^{-5} \pm 3.1 \times 10^{-5}$	$6.9 \times 10^{-5} \pm 4.3 \times 10^{-5}$
Ratio α/β	2.0×10^{-3}	5.7×10^{-5}	4.7×10^{-5}

Data represent means \pm standard deviation. Expression in one of the flank β -actin samples was assigned the value 1 and the RNA level in the rest of the samples is a fold-comparison with that sample. All samples are normalized to GAPDH expression level. Statistics: one-way ANOVA was used at significance level $\alpha=0.05$, followed by the Tukey multiple-comparison test. β -actin in flank, legs and wings: $p=0.25$; means are not significantly different. SMA expression in flank was significantly different ($p=0.00237$) from legs and wings. SMA expression in legs and wings was not significantly different.

for the flank tissue to be calculated. The active response manifests itself as a seemingly compression-stimulated rebound effect due to the explant pushing back, which causes an increase in the force required to maintain the fixed distance compression. Six independent samples of flank tissue were compressed and all of them exhibited this rebound response. Multiple compressions revealed that larger the initial compressive load on an individual sample the larger was the measured active response and in one case, the magnitude of the active response peak was larger than the initial compressive load (Fig. 5C). When flank tissue explants were treated with 1 μ M latrunculin A, an agent that specifically disrupts the actin cytoskeleton (Spector et al., 1989) for 30 min immediately prior to compression, the active response was eliminated (Fig. 5D). The surface tension of the latrunculin-treated flank tissue was not different from that of untreated flank (Fig. 3).

Expression of the α -smooth muscle actin (SMA) gene

The abrogation by latrunculin of the active response manifested by the flank, and its absence in the limb bud tissues (which behave in a classically viscoelastic fashion), suggested that the flank has unusual cytoskeletal properties. We hypothesized, therefore, that the active response of flank tissue might reflect an interaction between the flank cell membrane surface proteins with surrounding extracellular matrix molecules. Such an interaction allows for a globally coordinated force-stimulated signaling event which could lead to a muscle-like contraction of actin cytoskeletal elements within the flank cells. Fibroblasts under mechanical stress (Wang et al., 2000), or stimulation by TGF- β (Serini et al., 1998), for example, express the gene for SMA. The resulting actin cytoskeleton participates in a transmembrane linkage, termed the “fibronexus” (Singer, 1982), which mediates strengthened cell–matrix interactions (Wang et al., 2006).

We tested this hypothesis using quantitative real-time PCR (qPCR) on reverse transcripts of polyA(+) RNA isolated from E4 limb bud and flank tissues, to compare levels of SMA expression with that of non-muscle β -actin. Wing and leg each expressed similarly low levels of SMA, but the relative expression of this message by flank tissue was 30–40 fold greater than that of limb tissue (Table 3 and Fig. 6A). All the tissues expressed similar amounts of β -actin mRNA, however. Correspondingly, immunoblotting using an anti-SMA antibody showed substantial expression of this protein in flank tissue, but negligible amounts in limb tissues (Fig. 6B). Since limb budding in the embryo is initiated during the third day of development, we also assayed SMA expression in freshly isolated flank and limb field explants of E3 embryos. We found that expression of SMA was significantly lower in wing field than in flank tissue (Fig. 6C). Leg field mesenchyme, which lags slightly behind the wing field in producing a protrusive bud, also exhibited decreased levels of SMA RNA, but not significantly so (Fig. 6C). Similarly to the RNA expression results, SMA protein in the wing field in E3 embryos was lower than that in flank, but in the leg field it was roughly similar to the flank (Fig. 6D).

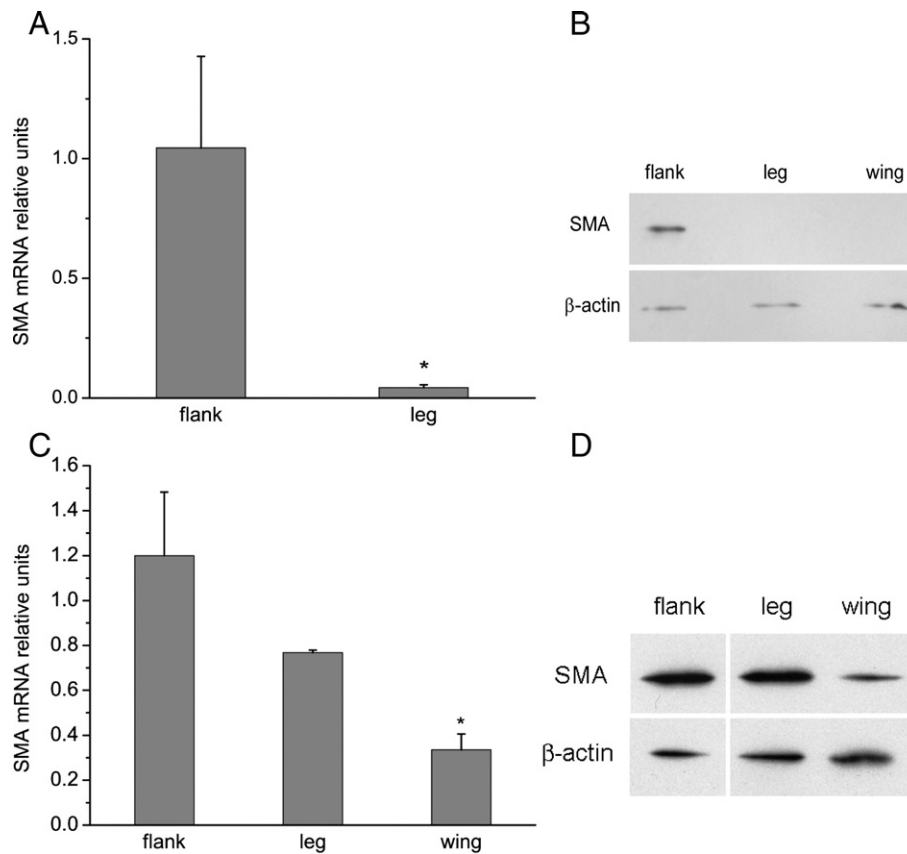


Fig. 6. (A) Relative SMA RNA expression in flank and legs of E4 embryos. Expression level in one flank sample was used as a normalizer and was set to one. Similar results were obtained for flank vs. wing (not shown). (B) Immunoblot analysis of SMA protein of flank, leg and wing buds from E4 embryos. Total protein amount was 28 μ g per lane. The upper blot was incubated with antibody against SMA. In the lower panel, from the same gel, β -actin was stained as a loading control. SMA was also abundant in flank explants and absent in wing and leg bud explants after overnight incubation, as used in the tensiometric analysis (not shown). (C) Relative SMA RNA expression in flank, leg and wing of E3 embryos. (D) Immunoblot analysis of SMA protein of flank, leg and wing buds from E3 embryos. Details were as in (B) except that 20, 22 and 28 μ g per lane were used, respectively for the flank, leg and wing samples. For qRT-PCR, * $p < 0.05$.

Visualization of SMA in limb and flank tissues of E4 embryos by immunofluorescence using an anti-SMA primary antibody confirmed the higher levels of expression of this cytoskeletal protein in flank than in both types of limb bud (Fig. 7). A high level of SMA staining extended through the entire thickness of the flank (Fig. 7, middle panels), the signal was most intense just beneath the embryo's surface ectoderm (lower region of section). Analysis of E3 embryos showed similar levels of immunoreactive SMA protein in all three tissues (not shown).

Ultrastructural differences between flank and limb bud cells

The ultrastructural features of the limb bud and flank cells of E4 embryos were generally similar (Fig. 8). Mesenchymal cells of both tissues contained large nuclei and narrow zones of cytoplasm with prominent rough endoplasmic reticulum and many cell processes. Despite their elevated levels of SMA, the flank cells did not contain the thick actin bundles seen in myofibroblasts (Tomasek et al., 2002). Strikingly, however, mesenchymal cells of the flank contained an irregularly arranged network of fine cytoplasmic microfilaments (mean of 60 measurements: 6.052 nm) (Fig. 8B). Although limb bud cells had a few visible microfilaments, no comparable networks were seen in wing (Fig. 8A) or leg mesenchyme.

E3 embryos showed comparable differences between limb and flank cells, although the apparently greater density of the mesenchymal cytoplasm at this stage made it difficult to discern cytoskeletal microfilaments in the central regions of the cells. When cell extensions were examined, however, networks and bundles of

microfilaments could be observed in flank cells (Fig. 8D) but were absent in limb cells (Fig. 8C).

Effects of FGF8

Implanting a bead soaked in FGF8 into the flank of an E3 chicken embryo between the wing and leg fields induces an ectopic limb bud, which develops into a limb with intermediate morphology between wing and leg (Ohuchi et al., 1995, 1998; Vogel et al., 1996). We found that E4 flank incubated in the presence of 25 ng/ml FGF8b was more cohesive than control flank incubated for the same period ($p < 0.003$), and similar in this property to limb, falling in between the wing and leg values (Fig. 3). Additionally, the active rebound response seen in normal flank tissue during the tensiometric experiments was largely abrogated by treatment with FGF8b (Fig. 4E).

The number of cells in flank tissue increased approximately 40–45% over 24 h in response to exposure to 25 ng/ml of FGF8b, whether incubation was performed in the presence of 10% FBS (as with the tensiometry experiments), or in the absence of this component (Fig. 9). The volume of the isolated tissue fragments appeared to be non-increasing over the culture period (not shown), suggesting that the cells became more densely packed in these flank explants in response to FGF8. However, this was not reflected in differences in the cell number density measured in specimens of flank tissues fixed after 24 h of incubation in the presence and absence of FGF8 (Table 2), possibly due to the aberrantly increased density of the mesenchymal tissues when fixed in the form of explants rather than in situ (see above). Interestingly, cell volume density, which decreased in incubated,

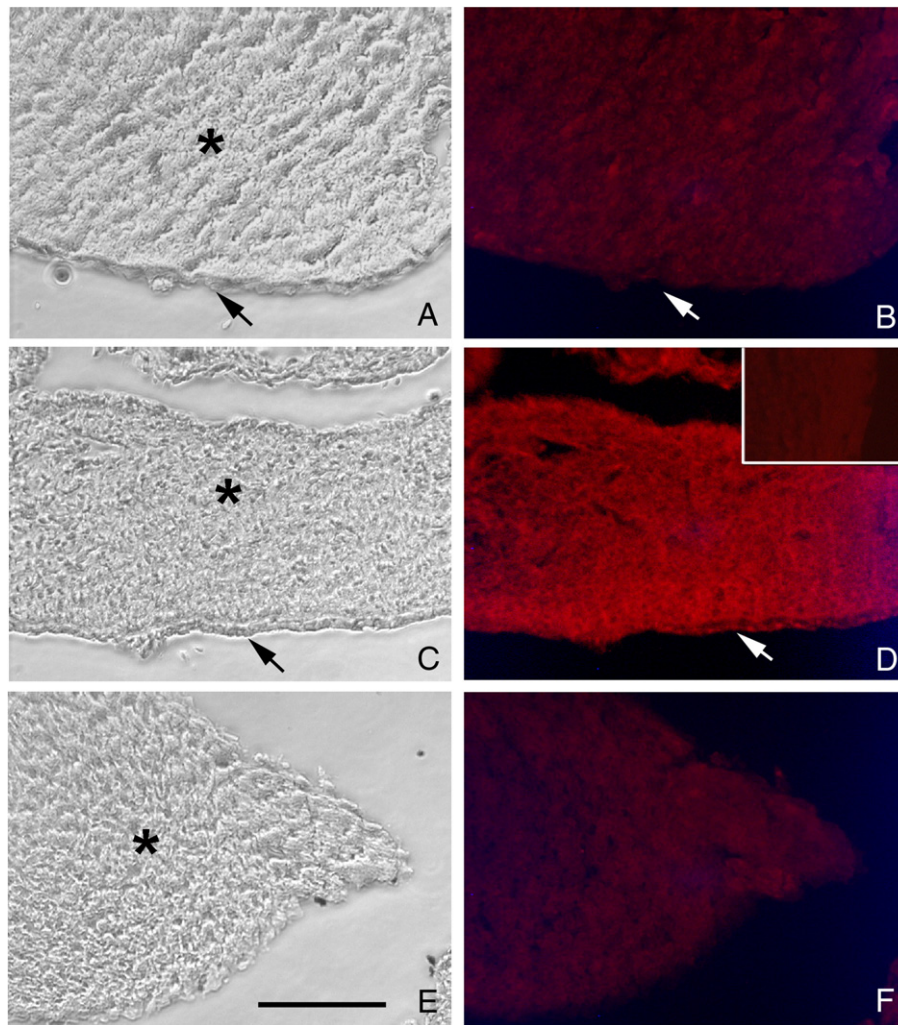


Fig. 7. Immunolocalization of SMA in wing bud, flank and leg bud of an E4 chicken embryo. Left panels, phase contrast images; right panels, corresponding immunofluorescent images: A and B, wing bud; C and D, flank; E and F, leg bud. Inset, flank no primary antibody control. Objective magnification 16 \times . All exposure times, including that of the inset, were the same. Asterisk: mesenchyme; arrow: ectoderm. Scale bar = 100 μ m.

relative to freshly isolated, flank did not do so when FGF8 was present (Table 2).

Treatment of flank tissue with FGF8 did not significantly change its level of expression of SMA RNA (not shown). Nonetheless, the microfilamentous network seen in flank tissue (Figs. 8B, D), while persisting in the untreated flank after incubation for 24 h (Fig. 10A), was not observed in flank cells that had been exposed to FGF8 (Fig. 10B). These results paralleled the tensiometric ones (Fig. 5), where the presence of FGF8 eliminated the rebound response.

Discussion

The above findings demonstrate that limb bud tissues have a larger surface tension, and are thus more cohesive, than the surrounding flank tissue in agreement with what can be termed the “limb budding by phase separation” proposal of Heintzelman et al. (1978). This proposal was based, in turn, on the more general Differential Adhesion Hypothesis (DAH) of Steinberg (Steinberg 1963, 1978, 1998), a morphogenetic principle that underlies many developmental and pathological processes (Godt and Tepass, 1998; Gonzalez-Reyes and St Johnston, 1998; Perez-Pomares and Foty, 2006). The DAH states that relative arrangements of cells within complex tissues, and tissues relative to one another within organs, can be predicted, under appropriate conditions, by the relative adhesive strengths of the

cells or cohesivities of the tissues, measured, respectively, on common quantitative scales.

Cohesivity differences in mesenchymal tissues, however, cannot have the same underlying cellular basis as in epithelioid tissues, the paradigmatic cases for the DAH. In epithelioid tissues, in which cells adhere to one another directly via cell adhesion molecules (CAMs), cohesivity differences can be attributed to different strengths of adhesion, which can be arranged on a quantitative scale regardless of which CAMs are involved. Mesenchymal tissues, in contrast, consist of cells embedded in an extracellular matrix (ECM). Cohesivity differences in mesenchymal tissues have been attributed to global network properties of ECM fibers (Forgacs et al., 1991, 2003; Newman, 1998; Newman et al., 2004) and cell–ECM interactions (Robinson et al., 2004), or both (reviewed in Forgacs and Newman, 2005). The present study suggests that an increased density of cells in limb buds vs. flank tissue, which is present both at 3 and 4 days of development (Fig. 4; Table 1), may account, in part, for the relatively higher values of cohesivity of limb bud tissues in E4 explants (Fig. 3). Treatment of flank with FGF8 increased its cohesivity (Fig. 3) and cell number (Fig. 9), during the incubation period, but induced differences in cell density could not unambiguously be determined (Table 2), possibly because of the contraction seen in the explants relative to intact embryonic tissue during fixation (Tables 1 and 2). This contraction would not pertain to the living tissues analyzed tensiometrically,

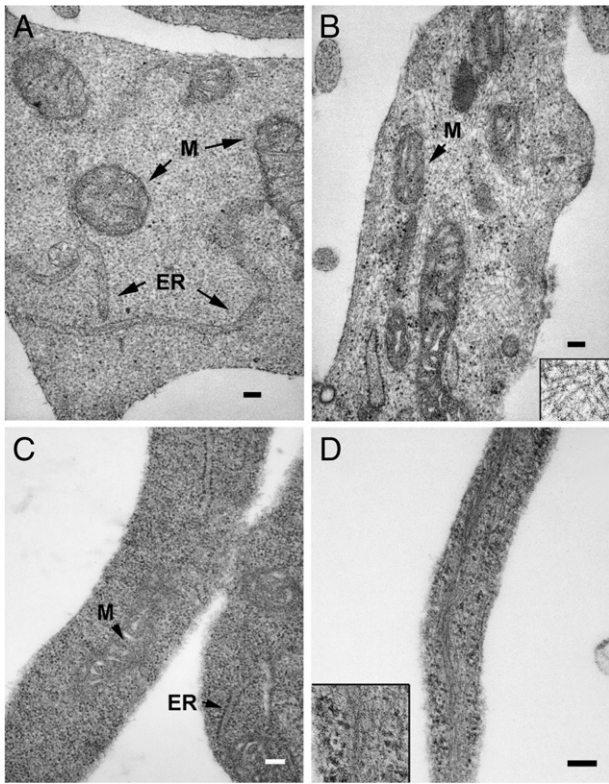


Fig. 8. Transmission electron micrographs of mesenchymal cells of wing buds and flanks of (A, B) E4 and (C, D) E3 embryos. (A) A mesenchymal cell of an E4 wing bud near the ectoderm, and (B), a mesenchymal cell of the E4 flank near the ectoderm. The flank cell contains a dense network of 6 nm microfilaments visible in sparse areas of its cytoplasm. M: mitochondria; ER: endoplasmic reticulum. Inset: Portion of flank cell cytoplasm digitally magnified 2 \times . (C) An extended portion of an E3 wing bud mesenchymal cell, and (D), an extended portion of an E4 flank mesenchymal cell. The flank cell contains numerous 6 nm filaments in both networks and oriented arrays. Inset: Portion of flank cell cytoplasm digitally magnified 2 \times . Scale bars=0.1 μ m.

however. Based on the morphometry of the embryonic tissues and the mitogenic effect on the flank of FGF8 we suggest that increase in cell density, in its own right, or by enhancing ECM connectivity, is one of the changes in limb field mesenchyme that promotes its individuation from the surrounding flank, and that increased density is reflected in higher tissue cohesivity.

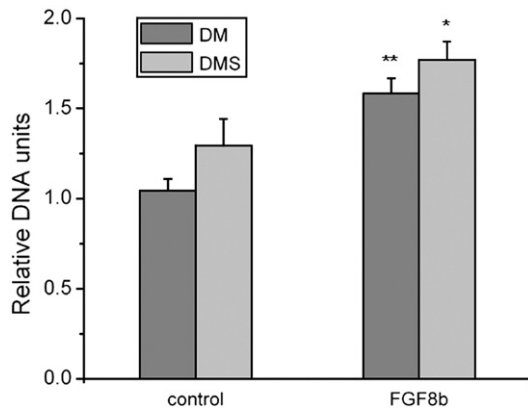


Fig. 9. DNA content of freshly isolated flank and flank incubated in 25 ng/ml FGF8b for 24 h. DNA was measured by qPCR using β -actin primers. See Materials and methods. $N=8$ for each treatment. Comparisons were between FGF8-treated flank and corresponding (i.e., serum-treated or untreated) controls. DM: serum-free defined medium; DMS: DM+10 fetal bovine serum. * $p<0.02$; ** $p<0.00005$.

Like a liquid droplet that phase separates from a second liquid of lower cohesivity with which it is immiscible, prospective limb bud tissues, if sufficiently more cohesive than flank tissue, would phase separate from the latter. Since the measured surface tension differences at E4 between both types of limb bud tissue and flank tissue are comparable to those of other embryonic tissues shown to be immiscible (Foty et al., 1996; Forgacs et al., 1998), our results (with the caveat that we could not directly ascertain limb and flank surface tensions at E3) support the hypothesis of Heintzelman et al. (1978) that tissue surface tension differences can lead to phase separation of the limb field from the flank, within which it originates.

In addition to the marked difference between limb and flank surface tensions we also found a difference in cohesivity between wing and leg mesenchyme, a result consistent with indirect assays of the properties of these tissues by Heintzelman et al. (1978) and Downie and Newman (1994). Since the two types of limb buds never confront one another in the course of development, this difference does not have a developmental implication analogous to the limb-flank distinction, but rather serves as a confirmation of the consistency of the various methods that have been used to assess tissue cohesivity.

Heintzelman et al. (1978) also proposed that not only the establishment of limb and flank as distinct, non-mixing tissues, but limb budding itself, can be explained by the different cohesivities of the tissues. In particular, the more cohesive tissue (limb) would assume a rounder morphology than the less cohesive tissue (flank)

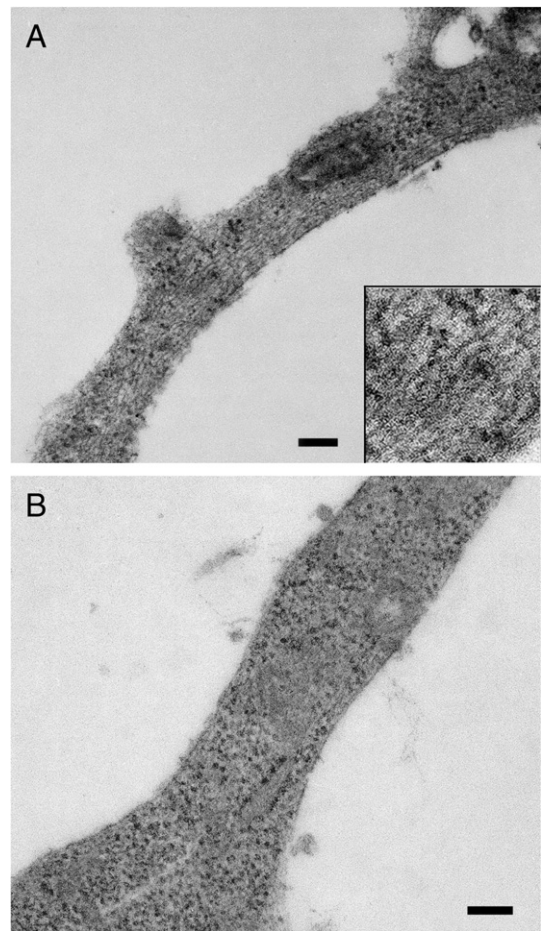


Fig. 10. Transmission electron micrographs of extended portions of mesenchymal cells from E4 flank explants that had been incubated for 24 h in (A) the absence, and (B) the presence of 25 ng/ml FGF8b. Protrusions of cells of the untreated flank continued to exhibit the dense network of 6 nm microfilaments seen in the E4 and E3 embryonic flank (see Fig. 8A), whereas organized microfilaments were not seen in any cell protrusions of the FGF8-treated flank tissue. Inset: Portion of untreated flank cell cytoplasm digitally magnified $\sim 4\times$. Scale bars=0.1 μ m.

with which it is embedded. Grima and Schnell (2007) have considered the question of whether surface tension differences can lead to morphogenetic changes such as the separation of adjacent somites from one another, or in the example considered here, the bulging of a limb bud from the flank. They demonstrate that several factors are involved in the plausibility of this mechanism for any given case: the magnitude of the surface tension differences of the adjoining tissues, the viscosity of the tissues, and the time course of the morphogenetic event (Grima and Schnell, 2007). Using quantitative physical arguments similar to those of these authors, we show in the Appendix that measured surface tension differences between E4 limb and flank tissues would indeed be sufficient to cause the change in contour of the limb bud relative to the flank seen during the initial 12 h of limb budding (Fig. 1, top left).

We do not know the precise function of the active response to compression seen in the flank tissue. A role for such behavior (characteristic of mechanically excitable media) in the initiation of morphogenetic changes has been proposed earlier (Odell et al., 1981; Belousov et al., 1994). In particular, Oster et al. (Odell et al., 1981; Davidson et al., 1995, 1999) suggested that the invagination of the vegetal plate at the onset of gastrulation in the sea urchin embryo is triggered by an active contractile response of the apical cortical actin cytoskeleton of cells in this region. The flank's active response may play a similar role. As the flank is rich in SMA it is also possible that the observed active response reflects a stiffening response similar to that found in *in vitro* cross-linked networks of actin filaments (Xu et al., 2000; Storm et al., 2005) and in cells in culture (Wang and Ingber, 1994; Deng et al., 2004; Icard-Arcizet et al., 2008).

The surface tension differential between the flank and limb tissues (again, assuming that what we have measured at E4 is also characteristic of the E3 tissues) assures that phase separation of the limb buds from the flank, and rounding up of the former within the latter, will occur. Rounding up of a more cohesive tissue that adjoins a less cohesive one is typically associated with the engulfment of the former by the latter (Steinberg and Poole, 1982; Armstrong, 1989). The limb bud actually protrudes from the flank during its budding, however, and it is here that the active response to compression seen in the flank tissue may come into play.

We suggest that as the prospective limb bud moves into the engulfing flank it exerts increasing pressure on it. As a consequence of the rebound effect, the resulting stress in the flank is not simply of the action–reaction type. It would lead instead to a force imbalance, a net force exerted by the flank on the limb, which may help to expel the latter from the former, resulting in budding. A prediction of this hypothesis is that disruption of the actin cytoskeleton of the flank tissue adjacent to the limb field, e.g., by latrunculin, would impair limb budding.

Interestingly, such an active response has never been noted in any previously published tensiometry measurements of either intact tissue explants or aggregated cells. Although it is dependent on an organized actin cytoskeleton (by evidence of its suppression by latrunculin; Fig. 3) it is not due to skeletal muscle, since the myoblasts that eventually give rise to body wall muscle have not reached the flank at E4 (Nowicki et al., 2003).

The high level of SMA gene expression in flank, relative to limb bud (Figs. 6 and 7; Table 3) provides a plausible basis for the active response, particularly in light of the extensive microfilamentous network seen in the flank cells (Fig. 8). This cytoskeletal protein, which is characteristic of smooth muscle and certain pathological contractile tissues (Wang et al., 2006), is not generally expressed at high levels in embryonic tissues apart from pericytes and the interesting case of the developing cardiac cushion mesenchyme (Sugi et al., 2004). We find that limb field tissue at E3 retains significant levels of SMA RNA and protein though its expression is beginning to decline, in wing earlier than in leg (Figs. 6C, D). Despite the fact that E3 limb tissues contain SMA protein, they do not exhibit the microfilamentous networks and bundles seen in flank cells (Fig. 9). Our finding that flank tissues

incubated in FGF8 lose their organized microfilaments suggests that this may also happen *in situ* in response to the AER, which secretes this factor. By E4 there is no detectable SMA protein in either wing or leg. It is clear that the progressive loss (and likely depolymerization) of SMA in the limb tissue is concomitant with limb budding. Although these phenomena are consistent with the expulsion hypothesis, above, additional evidence would be required to confirm this mechanism.

In summary, we suggest that changes in the “physical phenotype” induced in the limb field by the spatiotemporally regulated expression of FGF8 in the flank ectoderm is a major factor in the initiation of limb formation during development. Our tensiometric analysis of E4 limb and flank tissues (Figs. 3 and 4) provides insight into how this occurs: in particular, the greater surface tension of limb vs. flank mesenchyme, the rebound response of the flank, and the conversion of flank viscoelastic (Figs. 3 and 4) and cytoskeletal properties (Fig. 10) to those of limb by FGF8 provide plausible physical mechanisms for limb budding. The density differences between limb and flank tissue at both E3 and E4 (Fig. 4; Tables 1 and 2) and relative expression of SMA and organization of microfilaments (Fig. 6; Table 2) at E3 suggest that the physical, cellular and molecular differences between limb and flank seen at E4 also pertain to the period of limb budding.

We propose that the transformation of portions of the somatopleure into limb bud occurs in two partly overlapping stages. First, changes in cohesivity in the limb fields on or before E4 lead to phase separation of limb and flank tissue domains. Concomitantly, changes in the cytoskeleton of cells of the limb field (later in leg than in wing) lead to its surface tension-driven rounding up to occur in the context of surrounding flank tissue that, in contrast, retains its active mechanical properties. The flank's rebound response would thus promote the expulsion of the rounding buds. Since the resulting primordia constitute domains within which self-organization of skeletal structures can occur (Newman and Bhat, 2007; Newman et al., 2008), the physical transformations set off by the local elevation of FGF8 along the body wall ectoderm may also provide insight into the evolutionary innovation of the paired appendages (Newman and Müller, 2005).

Acknowledgments

We thank Jeff Swift and the Electron Microscopy Facility, Institute of Medical and Veterinary Sciences, Adelaide for assistance and resources; Dale Caville, Discipline of Pathology and Tavik Morgenstern, Discipline of Anatomical Sciences, University of Adelaide for help with photography. This work was supported by National Science Foundation grants EF-0526854 (G.F. and S.A.N.) and IBN-034467 (S.A.N.).

Appendix

If budding proceeds according to the laws of fluid dynamics then it is driven by interfacial forces and resisted by viscous forces. The first leads to energy gain, the latter to energy loss. In order to determine if interfacial forces indeed can be responsible for bud formation we need to estimate these two energy contributions. (For a similar analysis in another context see Newman et al., 1997).

As the limb bud forms from the flank, an interface develops between these tissues. This interface is energetically costly. We can think of the appearance of the bud as the continuous decrease of this interface. The loss of this interface occurs at the same rate as the increase of the forming bud. In mathematical terms (see Landau and Lifschitz, 1959, p. 54) we thus need to evaluate

$$\left| \sigma \frac{dA}{dt} \right| > \left| 2\eta \int_{ij} \left(\frac{\partial v_i}{\partial x_j} \right)^2 dV \right|. \quad (1)$$

The expression on the left is the rate at which energy is gained due to the loss of the flank–limb interface. Here σ is the flank–limb interfacial

tension, A is the instantaneous area (at time t) of the forming bud and $\partial A / \partial t$ denotes the derivative of A with respect to t . The expression on the right is the rate at which energy is dissipated due to viscous flow of the limb bud tissue. Here η is the viscosity of the tissue, v_i is the i th component of the flow velocity ($i, j = 1, 2, 3$; $v_1 = v_x$, $v_2 = v_y$, $v_3 = v_z$; $x_1 = x$, $x_2 = y$, $x_3 = z$) and integration is performed over the instantaneous volume of the forming bud.

The various terms in the above equation can conveniently be estimated. In the case of budding, the relevant time scale is $T_B \sim 12$ h (it takes about 12 h for the bud to assume a semicircular profile in which its proximodistal length is half its anteroposterior width) and the relevant length scale is $L_B \sim 10^{-2}$ cm (at time the bud has an oval base with long and short axis respectively of about 0.5 mm and 0.25 mm and protrudes about 0.25 mm from the flank). Thus expressing all entities in Eq. (1) in terms of L_B and T_B (i.e., $A: L_B^2$, $V: L_B^3$, $x: L_B$, and $v_B: L_B/T_B$), the inequality in Eq. (1) reduces to $\sigma/\eta > v_B$. A representative average value of the ratio σ/η for embryonic tissues, including chick limb, is 1.4×10^{-6} cm/s (see Gordon et al., 1972 and Grima and Schnell, 2007). Finally with the values of L_B and T_B quoted above, we conclude that in the case of bud formation the inequality is fulfilled (10^{-6} cm/s $>$ 10^{-7} cm/s) and thus surface tension forces are sufficient to drive this morphogenetic process.

In the case of somite formation (see Grima and Schnell, 2007), the analogous quantities are $T_Z: 10^3$ s, $L_Z: 10^{-3}$ cm, and thus $v_Z: 10^{-6}$ cm/s, which is of the same order of magnitude as σ/η . Thus, our analysis suggests that somites are unlikely to form exclusively through surface tension forces, a conclusion reached by Grima and Schnell (2007) using a different analysis.

References for Appendix

- Gordon, R., Goel, N.S., Steinberg, M.S., Wiseman, L.L., 1972. A rheological mechanism sufficient to explain the kinetics of cell sorting. *J. Theor. Biol.* 37, 43–73.
- Grima, R., Schnell, S. 2007. Can tissue surface tension drive somite formation? *Dev Biol* 307, 248–57.
- Landau, L.D., Lifshitz, E.M. 1959. *Fluid mechanics*. Pergamon Press, Oxford.
- Newman, S., Cloître, M., Allain, C., Forgacs, G., Beysens, D. 1997. Viscosity and elasticity during collagen assembly in vitro: relevance to matrix-driven translocation. *Biopolymers* 41, 337–347.

References

- Agarwal, P., Wylie, J.N., Galceran, J., Arkhitko, O., Li, C., Deng, C., Grosschedl, R., Bruneau, B.G., 2003. *Tbx5* is essential for forelimb bud initiation following patterning of the limb field in the mouse embryo. *Development* 130, 623–633.
- Armstrong, P.B., 1989. Cell sorting out: the self-assembly of tissues in vitro. *Crit. Rev. Biochem. Mol. Biol.* 24, 119–149.
- Belousov, L.V., Saveliev, S.V., Naumidi, I.I., Novoselov, V.V., 1994. Mechanical stresses in embryonic tissues: patterns, morphogenetic role, and involvement in regulatory feedback. *Int. Rev. Cytol.* 150, 1–34.
- Crossley, P.H., Minowada, G., MacArthur, C.A., Martin, G.R., 1996. Roles for FGF8 in the induction, initiation, and maintenance of chick limb development. *Cell* 84, 127–136.
- Davidson, L.A., Koehl, M.A., Keller, R., Oster, G.F., 1995. How do sea urchins invaginate? Using biomechanics to distinguish between mechanisms of primary invagination. *Development* 121, 2005–2018.
- Davidson, L.A., Oster, G.F., Keller, R.E., Koehl, M.A., 1999. Measurements of mechanical properties of the blastula wall reveal which hypothesized mechanisms of primary invagination are physically plausible in the sea urchin *Strongylocentrotus purpuratus*. *Dev. Biol.* 209, 221–238.
- Deng, L., Fairbank, N.J., Fabry, B., Smith, P.G., Maksym, G.N., 2004. Localized mechanical stress induces time-dependent actin cytoskeletal remodeling and stiffening in cultured airway smooth muscle cells. *Am. J. Physiol., Cell Physiol.* 287, C440–C448.
- Downie, S.A., Newman, S.A., 1994. Morphogenetic differences between fore and hind limb precartilaginous mesenchyme: relation to mechanisms of skeletal pattern formation. *Dev. Biol.* 162, 195–208.
- Duguay, D., Foty, R.A., Steinberg, M.S., 2003. Cadherin-mediated cell adhesion and tissue segregation: qualitative and quantitative determinants. *Dev. Biol.* 253, 309–323.
- Folkman, J., Moscona, A., 1978. Role of cell shape in growth control. *Nature* 273, 345–349.

- Foty, R.A., Pflieger, C.M., Forgacs, G., Steinberg, M.S., 1996. Surface tensions of embryonic tissues predict their mutual envelopment behavior. *Development* 122, 1611–1620.
- Forgacs, G., Newman, S.A., 2005. *Biological Physics of the Developing Embryo*. Cambridge Univ. Press, Cambridge.
- Forgacs, G., Newman, S.A., Obukhov, S.P., Birk, D.E., 1991. Phase transition and morphogenesis in a model biological system. *Phys. Rev. Lett.* 67, 2399–2402.
- Forgacs, G., Foty, R.A., Shafir, Y., Steinberg, M.S., 1998. Viscoelastic properties of living embryonic tissues: a quantitative study. *Biophys. J.* 74, 2227–2234.
- Forgacs, G., Newman, S.A., Hinner, B., Maier, C.W., Sackmann, E., 2003. Assembly of collagen matrices as a phase transition revealed by structural and rheologic studies. *Biophys. J.* 84, 1272–1280.
- Fung, Y.C., 1990. *Biomechanics: Mechanical Properties of Living Tissues*. Springer-Verlag, New York.
- Godt, D., Tepass, U., 1998. *Drosophila* oocyte localization is mediated by differential cadherin-based adhesion. *Nature* 395, 387–391.
- Gonzalez-Reyes, A.S., St Johnston, D., 1998. The *Drosophila* AP axis is polarised by the cadherin-mediated positioning of the oocyte. *Development* 125, 3635–3644.
- Grima, R., Schnell, S., 2007. Can tissue surface tension drive somite formation? *Dev. Biol.* 307, 248–257.
- Hamburger, V., Hamilton, H.L., 1951. A series of normal stages in the development of the chick. *J. Morphol.* 8, 49–92.
- Hegedüs, B., Marga, F., Jakab, K., Sharpe-Timmis, K.L., Forgacs, G., 2006. The interplay of cell–cell and cell–matrix interactions in the invasive properties of brain tumors. *Biophys. J.* 91, 1–9.
- Heintzelman, K.F., Phillips, H.M., Davis, G.S., 1978. Liquid-tissue behavior and differential cohesiveness during chick limb budding. *J. Embryol. Exp. Morphol.* 47, 1–15.
- Icard-Arcizet, D., Cardoso, O., Richert, A., Hénon, S., 2008. Cell stiffening in response to external stress is correlated to actin recruitment. *Biophys. J.* 94, 2906–2913.
- Israelachvili, J., 1992. *Intermolecular and Surface Forces*. Academic Press, London.
- Kawakami, Y., Capdevila, J., Buscher, D., Itoh, T., Rodriguez-Esteban, C., Izpisua-Belmonte, J.C., 2001. WNT signals control FGF dependent limb initiation and AER induction in the chick embryo. *Cell* 104, 891–900.
- Lewandoski, M., Sun, X., Martin, G.R., 2000. FGF8 signaling from the AER is essential for normal limb development. *Nat. Genet.* 26, 460–463.
- Livak, K.J., Schmittgen, T.D., 2001. Analysis of relative gene expression data using real-time quantitative PCR and the 2^{(-Delta Delta C(T))} method. *Methods* 25, 402–408.
- Mahmood, R., Bresnick, J., Hornbruch, A., Mahony, C., Morton, N., Colquhoun, K., Martin, P., Lumsden, A., Dickson, C., Mason, I., 1995. A role for FGF8 in the initiation and maintenance of vertebrate limb bud outgrowth. *Curr. Biol.* 5, 797–806.
- Min, H., Danilenko, D.M., Scully, S.A., Bolon, B., Ring, B.D., Tarpley, J.E., DeRose, M., Simonet, W.S., 1998. FGF10 is required for both limb and lung development and exhibits striking functional similarity to *Drosophila* branchless. *Genes Dev.* 12, 3156–3161.
- Moon, A.M., Capocchi, M.R., 2000. FGF8 is required for outgrowth and patterning of the limbs. *Nat. Genet.* 26, 455–459.
- Newman, S.A., 1998. Networks of extracellular fibers and the generation of morphogenetic forces. In: Beysens, D., Forgacs, G. (Eds.), *Dynamical Networks in Physics and Biology*. Springer-Verlag, Berlin, pp. 139–148.
- Newman, S.A., Comper, W.D., 1990. ‘Generic’ physical mechanisms of morphogenesis and pattern formation. *Development* 110, 1–18.
- Newman, S.A., Müller, G.B., 2005. Origination and innovation in the vertebrate limb skeleton: an epigenetic perspective. *J. Exp. Zool. B. Mol. Dev. Evol.* 304, 593–609.
- Newman, S.A., Bhat, R., 2007. Activator–inhibitor dynamics of vertebrate limb pattern formation. *Birth Defects Res. C Embryo Today* 81, 305–319.
- Newman, S.A., Forgacs, G., Hinner, B., Maier, C.W., Sackmann, E., 2004. Phase transformations in a model mesenchymal tissue. *Phys. Biol.* 1, 100–109.
- Newman, S.A., Christley, S., Glimm, T., Hentschel, H.G., Kazmierczak, B., Zhang, Y.T., Zhu, J., Alber, M., 2008. Multiscale models for vertebrate limb development. *Curr. Top. Dev. Biol.* 81, 311–340.
- Norotte, C., Marga, F., Neagu, A., Kosztin, I., Forgacs, G., 2008. Experimental evaluation of apparent tissue surface tension based on the exact solution of the Laplace equation. *Eur. Phys. J. Lett.* 81, 46003.
- Nowicki, J.L., Takimoto, R., Burke, A.C., 2003. The lateral somitic frontier: dorso-ventral aspects of antero-posterior regionalization in avian embryos. *Mech. Dev.* 120, 227–240.
- Odell, G.M., Oster, G., Alberch, P., Burnside, B., 1981. The mechanical basis of morphogenesis. I. Epithelial folding and invagination. *Dev. Biol.* 85, 446–462.
- Ohuchi, H., Nakagawa, T., Yamauchi, M., Ohata, T., Yoshioka, H., Kuwana, T., Mima, T., Mikawa, T., Nohno, T., Noji, S., 1995. An additional limb can be induced from the flank of the chick embryo by FGF4. *Biochem. Biophys. Res. Commun.* 209, 809–816.
- Ohuchi, H., Nakagawa, T., Yamamoto, A., Araga, A., Ohata, T., Ishimaru, Y., Yoshioka, H., Kuwana, T., Nohno, T., Yamasaki, M., Itoh, N., Noji, S., 1997. The mesenchymal factor, Fgf10, initiates and maintains the outgrowth of the chick limb bud through interaction with FGF8, an apical ectodermal factor. *Development* 124, 2235–2244.
- Ohuchi, H., Takeuchi, J., Yoshioka, H., Ishimaru, Y., Ogura, K., Takahashi, N., Ogura, T., Noji, S., 1998. Correlation of wing–leg identity in ectopic FGF-induced chimeric limbs with the differential expression of chick *Tbx5* and *Tbx4*. *Development* 125, 51–60.
- Perez-Pomares, J.M., Foty, R.A., 2006. Tissue fusion and cell sorting in embryonic development and disease: biomedical implications. *BioEssays* 28, 809–821.
- Robinson, E.E., Foty, R.A., Corbett, S.A., 2004. Fibronectin matrix assembly regulates $\alpha5\beta1$ -mediated cell cohesion. *Mol. Biol. Cell* 15, 973–981.
- Saito, D., Yonei-Tamura, S., Takahashi, Y., Tamura, K., 2006. Level-specific role of paraxial mesoderm in regulation of *Tbx5/Tbx4* expression and limb initiation. *Dev. Biol.* 292, 79–89.

- Sekine, K., Ohuchi, H., Fujiwara, M., Yamasaki, M., Yoshizawa, T., Sato, T., Yagishita, N., Matsui, D., Koga, Y., Itoh, N., Kato, S., 1999. FGF10 is essential for limb and lung formation. *Nat. Genet.* 21, 138–141.
- Serini, G., Bochaton-Piallat, M.L., Ropraz, P., Geinoz, A., Borsi, L., Zardi, L., Gabbiani, G., 1998. The fibronectin domain ED-A is crucial for myofibroblastic phenotype induction by transforming growth factor-1. *J. Cell Biol.* 142, 873–881.
- Shaw, T., Winston, M., Rupp, C.J., Klapper, L., Stoodley, P., 2004. Commonality of elastic relaxation in biofilms. *Phys. Rev. Lett.* 93, 098102–098191.
- Singer, I.L., 1982. Association of fibronectin and vinculin with focal contacts and stress fibers in stationary hamster fibroblasts. *J. Cell Biol.* 92, 398–408.
- Spector, I., Shochet, N.R., Blasberger, D., Kashman, Y., 1989. Latrunculins — novel marine macrolides that disrupt microfilament organization and affect cell growth: I. Comparison with cytochalasin D. *Cell Motil. Cytoskeleton.* 13, 127–144.
- Steinberg, M.S., 1963. Reconstruction of tissues by dissociated cells. Some morphogenetic tissue movements and the sorting out of embryonic cells may have a common explanation. *Science* 141, 401–408.
- Steinberg, M.S., 1978. Specific cell ligands and the differential adhesion hypothesis: how do they fit together? In: Garrod, D.R. (Ed.), *Specificity of Embryological Interactions*. Chapman and Hall, London, pp. 97–130.
- Steinberg, M.S., 1998. Goal-directedness in embryonic development. *Integr. Biol.* 1, 49–59.
- Steinberg, M.S., Poole, T.J., 1982. Liquid behavior of embryonic tissues. In: Bellairs, R., Curtis, A.S.G. (Eds.), *Cell Behavior*. Cambridge University Press, Cambridge, pp. 583–607.
- Storm, C., Pastore, J.J., MacKintosh, F.C., Lubensky, T.C., Janmey, P.A., 2005. Nonlinear elasticity in biological gels. *Nature* 435, 191–194.
- Sun, X., Mariani, F.V., Martin, G.R., 2002. Functions of FGF signalling from the apical ectodermal ridge in limb development. *Nature* 418, 501–508.
- Sugi, Y., Yamamura, H., Okagawa, H., Markwald, R.R., 2004. Bone morphogenetic protein-2 can mediate myocardial regulation of atrioventricular cushion mesenchymal cell formation in mice. *Dev. Biol.* 269, 505–518.
- Tanaka, M., Tickle, C., 2004. Tbx18 and boundary formation in chick somite and wing development. *Dev. Biol.* 268, 470–480.
- Tomasek, J.J., Gabbiani, G., Hinz, B., Chaponnier, C., Brown, R.A., 2002. Myofibroblasts and mechano-regulation of connective tissue remodelling. *Nat. Rev., Mol. Cell Biol.* 3, 349–363.
- Vogel, A., Rodriguez, C., Izpisua-Belmonte, J., 1996. Involvement of FGF8 in initiation, outgrowth and patterning of the vertebrate limb. *Development* 122, 1737–1750.
- Wang, N., Ingber, D.E., 1994. Control of cytoskeletal mechanics by extracellular matrix, cell shape, and mechanical tension. *Biophys. J.* 66, 2181–2189.
- Wang, J., Seth, A., McCulloch, C.A., 2000. Force regulates smooth muscle actin in cardiac fibroblasts. *Am. J. Physiol., Heart Circ. Physiol.* 279, H2776–2785.
- Wang, J., Zohar, R., McCulloch, C.A., 2006. Multiple roles of α -smooth muscle actin in mechanotransduction. *Exp. Cell Res.* 312, 205–214.
- Weibel, E.R., Kistler, G.S., Scherle, W.F., 1966. Practical stereological methods for morphometric cytology. *J. Cell Biol.* 30, 23–38.
- Xu, X.L., Weinstein, M., Li, C.L., Naski, M., Cohen, R.I., Ornitz, D.M., Leder, P., Deng, C.X., 1998. Fibroblast growth factor receptor 2 (FGFR2)-mediated reciprocal regulation loop between FGF8 and FGF10 is essential for limb induction. *Development* 125, 753–765.
- Xu, J.Y., Tseng, Y., Wirtz, D., 2000. Strain hardening of actin filament networks—regulation by the dynamic cross-linking protein α -actinin. *J. Biol. Chem.* 275, 35886–35892.